Fabrication of graphene: CdSe quantum dots/CdS nanorod heterojunction photodetector and role of graphene to enhance the photoresponsive characteristics

Chandrasekar Perumal Veeramalai (pv_chandrasekar@yahoo.com)
Minzu University of China

Pratap kollu
University of Hyderabad

Guochen Lin
Minzu University of China

Xiaoming Zhang
Minzu University of China

Chuanbo Li
Minzu University of China

Research Article

Keywords: CdSe QDs, graphene, CdS nanorods, heterojunction, photodetector

Posted Date: February 11th, 2021

DOI: https://doi.org/10.21203/rs.3.rs-231208/v1

Version of Record: A version of this preprint was published at Nanotechnology on May 10th, 2021. See the published version at https://doi.org/10.1088/1361-6528/abf87a.

Fabrication of graphene: CdSe quantum dots/CdS nanorod heterojunction photodetector and role of graphene to enhance the photoresponsive characteristics

Chandrasekar Perumal Veeramalai[*a], Pratap kollu[b], Guochen Lin[a], Xiaoming Zhang[a], Chuanbo Li*[a,c]*

[a]School of Sciences, Minzu University of China, Beijing 100081, China
[b]CASEST, School of Physics, University of Hyderabad, Prof. C.R. Rao Road, Gachibowli, Hyderabad -500046, India
[c]Optoelectronics Research Center, Minzu University of China, Beijing 100081, China
E-mail: Corresponding author: cbli@muc.edu.cn, pv_chandrasekar@yahoo.com

Integration of graphene with semiconducting quantum dots (QDs) provides an elegant way to access the intrinsic properties of graphene and optical properties of QDs in a single hand to realize the high-performance optoelectronic devices. In the present study, high-performance photodetector based on graphene: CdSe QDs/CdS nanorod heterostructures, are demonstrated. The resulting heterojunction photodetector with device configuration ITO/graphene: CdSe/CdS nanorods/Ag show excellent operating characteristics including a maximum photoresponsivity of 15.95 AW^{-1} and specific detectivity of 6.85×10^{12} Jones measured at 530 nm. The device exhibits a photoresponse rise time of 545 ms and a decay time of 539 ms. Furthermore, the effect of graphene nanosheets on the performance enhancement of heterojunction photodetector was explored. The results indicate that, due to the enhanced energy transfer from photoexcited QDs to graphene layer, light absorption is increased and excitons are generated. Also, the graphene: CdSe QDs/CdS nanorod interface can facilitate charge carrier transport effectively. This work provides a promising approach to develop high-performance visible-light photodetectors and utilization of advantageous features of graphene in optoelectronic devices.

Keywords: CdSe QDs; graphene; CdS nanorods; heterojunction; photodetector

1. Introduction

Graphene nanosheets, a honeycomb structured carbon material, possess unique properties like high thermal stability, mechanical strength, and excellent electrical conductivity[1,2]. By virtue of its distinct characteristics, attention was drawn to represent graphene in the development of novel devices which can be used in various applications spanned from electronics to the medical field[3-5]. However, the zero-band gap nature of graphene restricts its application in optoelectronic devices effectively. This obstacle could be overcome by the modification of graphene surface with metals, metal oxides, quantum dots, and will further broaden the application field with tunable properties[6-8].

Meanwhile, semiconductor QDs are zero-dimensional materials exhibits unique optical and electrical properties due to their small size of 2–10 nm[9, 10]. With the inherent fascinating properties, semiconducting QD has potential applications in photodetectors, solar cells, bio-imaging, and many more[11-13]. Nevertheless, graphene and semiconducting QDs also have their disadvantages. For instance, the de-coherence and low carrier mobilities limit the optical gain of QD materials. And also, the low light absorption, ultra-fast recombination of photogenerated carriers, and ease of aggregation in solution restrict the graphene application in optoelectronic devices[14]. Therefore, in recent years, there has been renewed interest in the integration of graphene with nanoparticles. In the graphene nanocomposite structure, the semiconducting nanoparticles act as a light-absorbing layer to produce electron-hole pairs, and then, charge carriers are rapidly transferred through high mobility graphene layers[15]. Moreover, it is possible to extend the QDs emission to longer wavelengths by combining the electronic properties of graphene with those of QDs in graphene: QD nanocomposites [16]. One of the important issues in the attachment of QDs on the surface of graphene is the monodispersity, which is essential for controlled charge transfer across the graphene layers.

Therefore, many efforts were devoted to synthesizing graphene-QD hybrid structures and designing photoelectric devices. For example, Geng *et al.* demonstrated the non-covalent attachment of CdSe QDs to graphene to realize highly transparent semiconducting films[17]. Guo *et al* have developed a strategy to fabricate a solar cell using CdSe QDs-graphene and achieved the incident photon-to-charge-carrier conversion efficiency (IPCE) of 16%, a large improvement from the graphene-only and QD-only devices (IPCE<6%)[15]. The decoration of CdSe QDs on graphene sheets and the effect of graphene inclusion on optoelectronic properties of the QD based device was investigated by Kim *et.al*[18]. Sun *et al.* have reported the CVD-grown monolayer graphene-PbS QDs based flexible infrared photodetector on plastic substrates and the device has shown enhanced photoresponsivity of 10^7 AW^{-1}[19]. Recently, Chen *et al.* proposed a photodetector of intercalated graphene layers with thick PbS QDs films (i.e. alternating layers of QDs and graphene) and achieved the efficient charge collection over the spectral range from visible to IR region[20]. by adopting the advanced technique of ink-jet printing, cook *et al.* have fabricated ZnO/graphene nanoplatelet bulk heterojunction UV photodetector and its photoresponsivity value reaches up to 2.2 AW^{-1}[21]. Furthermore, charge carrier dynamics of nanoparticle (quantum dots)/graphene nanocomposites also have been studied experimentally and theoretically[22-25]. Specifically, the photoluminescence of CdSe QDs in graphene nanohybrids is reduced both in intensity and lifetime due to strong interaction and energy transfer[26]. These above-mentioned works highlight the importance of graphene's role to enhance the charge carrier dissociation and transport in the optoelectronic device. However, to the best of our knowledge, only a little research is reported on the effect of graphene in heterojunction photodetectors. For instance, Konstantatos *et al.* demonstrated monolayer or bilayer graphene-PbS QDs heterojunction phototransistor, where trapped charges at the interface causing a photogate effect and enhance the device

photoresponsivity up to 10^7 AW^{-1} which is significantly higher than graphene only device of 10^{-2} AW^{-1}[27]. Therefore, there is an immediate need for studying the optoelectronic properties of graphene: QD nanocomposites and specifically, the role of graphene on performance metrics of optoelectronic devices.

Herein, we present the hybrid photodetector consists of graphene: CdSe QDs and CdS nanorod. The graphene: CdSe QDs nanocomposite was synthesized via low-temperature in-situ synthesis technique. The PL and TRPL studies of graphene: CdSe QDs nanocomposite showed an obvious quenching effect compared to the pure CdSe QDs as the reason for fast separation and transfer of photo-induced charge carriers between CdSe QDs and graphene layers. The as-fabricated hybrid heterojunction photodetector with device structure ITO/graphene: CdSe QDs /CdS/Ag shows enhanced photo responsivity of 15.95 AW^{-1} and specific detectivity of 6.85×10^{12} Jones which is significantly higher than ITO/CdSe/CdS/Ag device. Our work demonstrates the great potential of graphene: QD nanocomposite as the photoactive layer in the high-performance photodetector.

2. Experimental methods

2.1 Materials: All reagents were the technical grade of high purity, is used without further purification.1-Octadecene ($C_{16}H_{36}$, purity 99.0%) and Trioctylphosphine ($C_{24}H_{51}P$, purity >95.0 %), were purchased from Aladdin Industrial Corporation, Shanghai, P.R.China. n-Octylamine ($C_8H_{19}N$, purity > 99.0 %), Selenium powder (Se, purity ~ 99.0 %), Cadmium acetate dihydrate ($C_4H_5CdO_4.2H_2O$, purity ~ 98.0%) and oleic acid were purchased from Sinopharm Chemicals reagents. Co.Ltd. Graphene powder is purchased from alfa nano Inc. Shangai, P.R.China.

2.2 Preparation of graphene solution

For typical preparation of graphene solution, 5 mg of graphene powder was dissolved in 5 ml of 1-Octadecene (1mg/ml) and sonicated for 4 hr. The resulting solution is centrifugated for 5 min at 2000 rpm. The supernatant was collected and the process is repeated at 4000, 6000, 8000, and 10,000 rpm to get single-layer graphene in ODE solution. The final concentration of graphene: ODE solution is 0.13 mg/ml.

2.3 In-situ synthesis of CdSe QD-Graphene

The CdSe QDs were synthesized according to the reported literature with slight modification [28]. In a typical synthesis, the precursors are prepared in the following way. Cadmium precursor: 0.4mM of cadmium acetate dihydrate is taken in the round bottom flask and 10 ml of 1-octadecene, 0.250 ml of oleic acid, 1 ml of graphene solution, and 1 ml of n-octylamine is added. And then, the mixture is stirred for 30 min at 130 ℃. Selenium precursor: 2 mM metallic selenium powder is dissolved in 6 ml of tri-octyl phosphine (TOP) and 1.8 mL of toluene. For the CdSe QDs-graphene growth, 2 ml of selenium-TOP solution was injected into the reaction flask containing cadmium precursor, and the reaction mixture was kept at 170 ℃. For pristine CdSe QDs growth, the procedure is followed as the same, but without graphene solution added to the cadmium precursor. The samples were taken at different time intervals of 5, 10, 15, 20, and 30 min. The samples were purified with hexane/ methanol solution and precipitated by centrifugation at 10,000 rpm with acetone. The precipitated colloidal powder is dried and dissolved in hexane, toluene, or chloroform.

2.4 Synthesis of CdS nanorods

In a typical procedure, 20 mM cadmium acetate was dissolved in 25 ml of DI water. Then 0.250 ml of TGA was added under vigorous stirring at room temperature. Further, sulfur source solution was prepared by dissolving 40 mM sodium sulfide dihydrate in 50 ml of DI water and

added with cadmium source solution. The resulting mixture was stirred for 30 min and transferred into a 100 ml Teflon-lined stainless-steel autoclave. The autoclave was maintained at 180 ℃ for 8 hr and then cooled to room temperature naturally. After cooling to room temperature, the precipitation was washed with DI water and absolute ethanol several times to remove the excess reactants and byproduct. Finally, the sample was dried in a vaccum oven at 40 °C overnight.

2.5 Photodetector fabrication and Characterization

Firstly, the pre-patterned ITO glass substrate was cleaned with detergent, deionized (DI) water, isopropyl alcohol, and acetone for 15 min using ultra-sonication. Further, substrates were treated with UV ozone to make the surface hydrophilic. The as-synthesized CdS NRs solution (10mg ml-1 in n-butanol) was drop-casted on ITO glass substrates and dried at 80 ℃ for 5 min. The CdSe QDs or graphene-CdSe QDs in n-hexane (100 mg/ ml) was spin-coated at 1000 rpm for 6 s and 3000 rpm for 60 s and then samples were treated with ethanol washing twice. Finally, a vacuum evaporated Ag electrode (80 nm) was deposited to complete the device fabrication.

The UV-visible absorption spectra of as-synthesized CdSe QDs and graphene:CdSe QDs samples were analyzed on UV/vis/NIR spectrophotometer (Shimadzu, UV-3600). The steady-state photoluminescence (PL) spectra were acquired by using a fluorescence spectrophotometer (Hitachi, F-4600). Raman spectra of samples were taken at room temperature using 514.5 nm incident photons from an Ar ion laser (JY LabRam) in a backscattering geometry. The surface morphology of samples were acquired by a ZEISS sigma 500 field emission scanning electron microscopy (SEM) at 30kV. A Philips CM200 tunneling electron microscope (TEM) operating at an accelerating voltage of 200 kV, with a Bruker SDD EDX system was used for transmission electron microscopy studies. The FTIR spectra of the samples were recored in a NICOLET 10

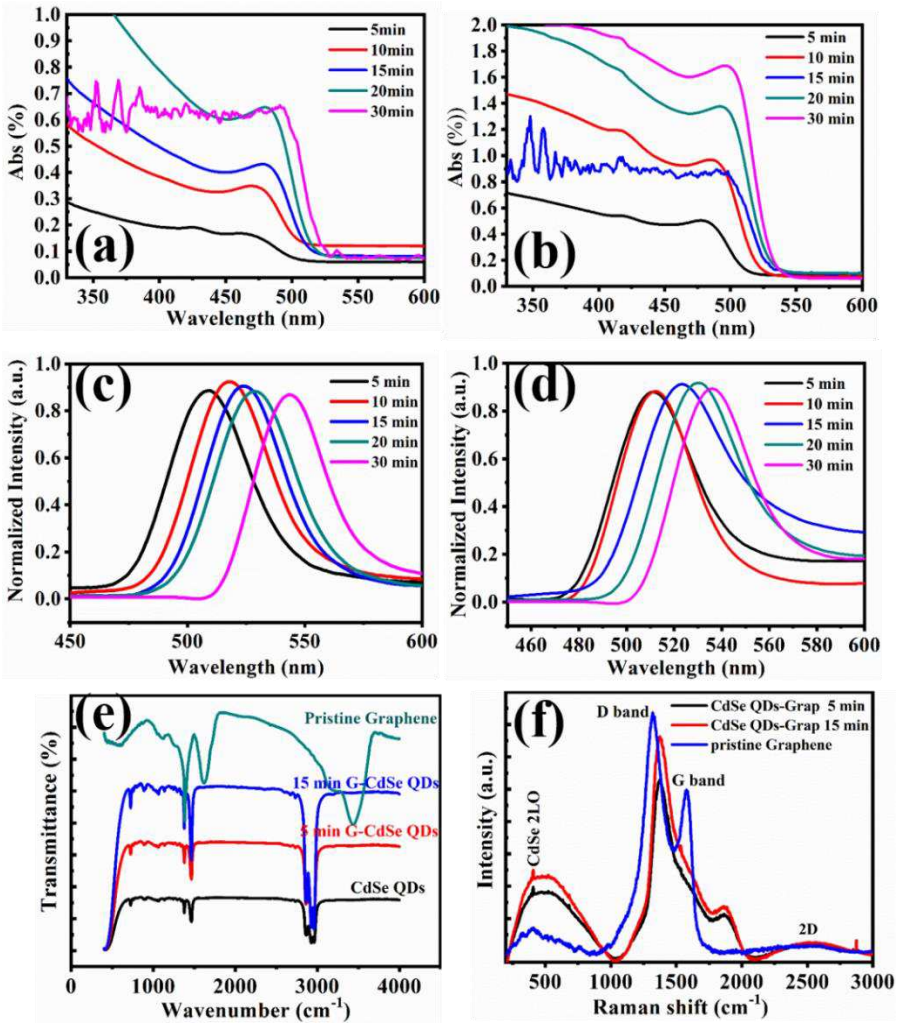

Figure.1 UV-visible absorption spectra spectra of (a) CdSe QDs (b) graphene:CdSe QDs. Photoluminescence spectra of (c) CdSe QDs (d) graphene:CdSe QDs. (e) FTIR spectra of pure CdSe QDs, graphene: CdSe QDs synthesized for 5 min, graphene: CdSe QDs synthesized for 15 min, and pure graphene. (f) Raman spectra of the pristine graphene, graphene: CdSe QDs synthesized for 5 min, and graphene: CdSe QDs synthesized for 15 min.

spectrometer operating in the range of 4000 to 400 cm^{-1}. All the electrical parameters of devices were measured by the Keithley 4200-SCS semiconductor characterization system assisted with a probe station. The irradiation was generated from monochromatic light-emitting diodes (530 nm), while the power of the incident radiation was tuned and measured with a power meter (Sanwa

Mobiken LASER POWER METER LP1). All the measurements were done in air at room temperature.

3. Results and Discussion

The as-synthesized CdSe QDs and graphene: CdSe QDs diluted in hexane solution under UV illumination are shown in **Figure S1(Supporting Information)**. Photographic image of the CdSe QDs and graphene: CdSe QDs nanocomposites synthesized with different reaction times under UV light irradiation at 365nm shows that the samples emit different colored light indicative of the size-tunable formation of QDs with time variable. **Figure 1(a)** presents the UV-Vis absorption spectra of pristine CdSe QDs and graphene: CdSe QDs nanocomposite, which clearly showed the excitonic absorption edge was red-shifted as reaction time prolongs. For CdSe QDs synthesized for 5 min would show the absorption peak at 468 nm. Subsequently, the absorption peaks were shifted to 493 nm for the sample synthesized for 30 min. Compared with bulk CdSe, blue shifting of peaks indicated the emergence of the quantum confinement effect. However, the absorption spectra of graphene: CdSe QDs as in Figure1(b) showed a slight red shifting compared to pure CdSe QDs. It should be noted that graphene had no obvious absorption characteristics in the visible region; the visible light absorption was due to the contribution of CdSe QDs. The absorption spectra were changed from 479 nm to 498 nm for samples of 5 min to 30 min respectively.

The photoluminescence spectra of the pure CdSe QDs and graphene: CdSe QDs nanocomposites were displayed in Figure 1(c,d). As shown in Figure1(c), an obvious emission peak at 510 nm was observed for pure CdSe QDs synthesized for 5 min and it shifts towards a higher wavelength as the synthesis time prolongs. At most, CdSe QDs synthesized for 30 min would show the emission peak at 535nm. It could be understood that the shifts might be related to the quantum confinement effect as the size of QD evolves. However, for graphene: CdSe QDs

nanocomposite, the emission peaks were observed at 512, 518, 526,533, and 543 nm for 5, 10, 15, 20- and 30-min samples respectively as shown in **Table.S2 (SI)**. Since there is no contribution of size of QDs to shifting of emission peak, we believe that this shifting would come from photoluminescence quenching effect.

Figure 1(e) presents the FTIR spectra of CdSe QDs capped with oleic acid and graphene: CdSe QDs synthesized for 5 min and 15 min. It is found that there is no peak observed at > 3000 cm^{-1} as compared to TOPO capped CdSe QDs. Typical features of the Cd-Se band stretching can be observed at 724 cm^{-1}. All other peaks are structural bonding of oleic acid with cadmium selenide QDs i.e 1378, 1466, 2861, 2873, 2931, and 2960 cm^{-1}. The CH_3 and CH_2 bending deformed behavior can be observed at 1378 and 1466 cm^{-1} respectively. All these above observations indicated evidently that CdSe QDs were attached on the surface of graphene successfully.

Raman spectroscopy was used to characterize the ordered disordered crystal structures of carbon materials. To generalize the scheme, CdSe QDs-graphene samples synthesized for 5 min and 15 min were characterized for Raman spectra in sense of the different sizes of QDs on a graphene sheet. Raman spectra of pristine graphene sheets were also given for comparison. As indicated in Figure1(f), all three samples were exhibited the characteristic phonon modes of vibration on laser excitation. For pristine graphene sheet, two peaks at 1319.8 cm^{-1} and 1580.4 cm^{-1} were observed and assigned to characteristic D and G bands of the two-dimensional carbon layer. Besides, a broad low-intensity peak also appears at 2500 cm^{-1} represents the 2D band of graphene. However, for the CdSe QDs functionalized graphene, an obvious characteristic peak of D and G bands are appeared along with a clear peak at 403 cm^{-1} which represents the overtone LO mode termed as CdSe 2LO[29]. In general, the D band at 1357 cm^{-1} is the breathing mode of π-point phonons of A_1g symmetry attributed to local defects and disorders, particularly the defects located

at the edges of graphene. And also, the G band is assigned to the E_2g phonon of sp2 bonds of carbon atoms. After depositing QDs on the graphene, significant red shifting of D and G bands were observed for QD-graphene hybrids synthesized at 5 min and 15 min. A redshift of D band by 55 cm^{-1} and 63 cm^{-1} were observed for 5 min and 15 min samples respectively. On the other hand, redshifts of G band by 277 cm^{-1} and 279 cm^{-1} were observed for 5 min and 15 min samples respectively. The G band shifting can be affected by the carrier doping levels, strain, and localized temperature[30-32]. Here, unlike the D band, the G band has shifted significantly concluded that charge transfer from QD functionalization and subsequent strain occurred by QDs loading on the graphene layer.[22] In addition to the redshifting of characteristic peaks, the intensity ratio I_D/I_G as shown in **Figure S2(a) (** in **SI)** also provides the degree of QDs functionalization on graphene layers. After QDs deposition on graphene, the I_D/I_G increases from 1.47 for pristine graphene to 4.69 for graphene-QDs of 15 min. Moreover, as shown in **Figure S2(b) (**in **SI)**, an enhancement of I_{2D}/I_G ratio was observed, which suggests the presence of a QDs on the graphene layers.

Furthermore, the photo-induced kinetics of graphene: CdSe QDs are analyzed by time-resolved photoluminescence (TRPL) spectroscopy. TRPL was employed to test the emission lifetime of pure CdSe QDs (5 min), graphene: CdSe QDs (5 min), and graphene: CdSe QDs (15 min) samples using 585 nm excitation wavelength **(see Figure S3 in the SI)**. A tri-exponential decay model was used to fit the decay curve: $(t) = A_1 e^{-t/\tau_1} + A_2\, e^{-t/\tau_2} + A_3\ e^{-t/\tau_3}$, where I(t) is the time-dependent fluorescence intensity, A is the amplitude and τ is the lifetime. The emission lifetime of measured samples is summarized in **Table S1 (**in **SI)**. It is noted that the average emission lifetime (τ_{ave}) of graphene: CdSe QDs nanocomposites was relatively shorter than that of the corresponding pure CdSe QDs. The average lifetime of CdSe QDs is calculated to be 557.9 ns and graphene: CdSe QDs (5 min) is 128.34 ns. Here, it should be considering the fact that the as-

synthesized CdSe QDs are used for the measurement and device application without ligand-exchange process. Therefore, the long-chain hydrocarbon oleic acid ligand used for the initial synthesis process form an insulating layer around each QD. Consequently, the organic ligands create an energetic barrier to charge transport[33]. However, the difference in the average lifetime between pure CdSe QDs and graphene: CdSe QDs indicates the existence of a non-radioactive pathway from the electronic interaction between quantum dots and graphene[34, 35].

The TEM and HRTEM images of representative CdSe QDs and graphene-CdSe QDs synthesized for 15 min were depicted in Figure 2. As in Figure 2 (a), CdSe QDs show a uniform size distribution with good crystalline quality. The size of the CdSe QD was in the range of 2 - 2.3

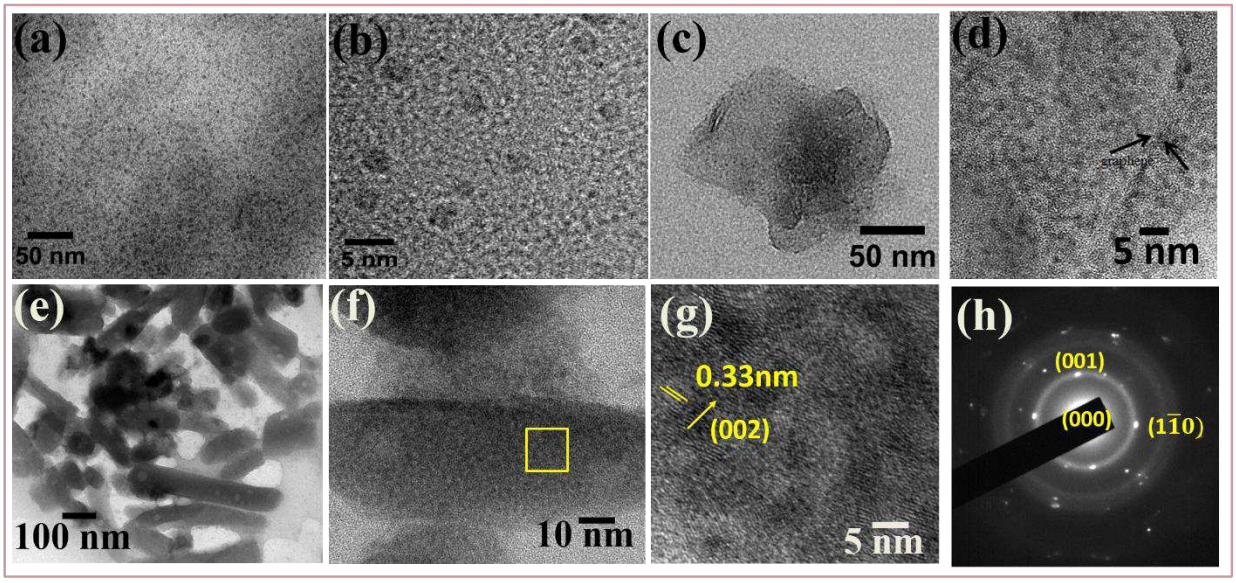

Figure.2 (a) Low magnified TEM image of CdSe QDs. (b) High magnification TEM image of CdSe QDs. (c) HRTEM image of graphene-CdSe QDs nanocomposite. (d) high magnification HRTEM image of graphene- CdSe QDs. (e) Low magnification TEM image of CdS nanorods. (f) high magnification TEM image of CdS nanorod. (g) the enlarged portion of the selected area in CdS nanorods (yellow square in Figure2(f)). (h) selected area electron diffraction (SAED) pattern of CdS nanorods.

nm as calculated from the HRTEM image for the sample synthesized for 15 min, which is consistent with that of absorption spectra measurement. The existence of clear lattice planes on the HRTEM as in Figure 2 (b) represents the good crystallization of CdSe QDs. It is also indexed to the cubic phase of CdSe with the lattice constant of a=0.62 nm. Interestingly, synthesis of QDs in presence of graphene would show a more pronounced growth compared with pure QD synthesis. As could be seen in Figure 2(c, d), the CdSe QDs randomly attached with graphene and highly loaded on the surface of graphene. It is appeared to be clearer in shape with lattice fringes along (100) plane dominated. It seems to be the same size distribution of CdSe QDs on graphene as pure CdSe QDs. The results supported the argument that the redshifting of absorption spectra was not from the size tuning of QDs. The red shifting of absorption spectra might be from the chemical interaction of QDs on the face of graphene due to charge delocalization [36].

The phase purity and the crystal structure of the hydrothermally synthesized CdS nanorods are investigated by powder X-ray diffraction (PXRD). As shown in **Figure S4 (**in **SI)**, the strong peaks indicate that the crystallinity of the product is good and no intensities of source materials or impurities are found in the spectrum. And also, the analysis of CdS data exhibits the lattice parameter of a=4.123 Å and c=6.686 A which agrees with the reported literature [37, 38]. The XRD pattern exhibits prominent, broad peaks at 2θ values of 31.5, 35.2°, 41.6°, 50.7°, 60.4° which could be indexed to scattering from 200, 102, 102,110,112 and 104 planes respectively. The XRD shows the presence of both cubic and hexagonal phases in the synthesized CdS nanorods, which is unusual in CdS crystal growth [39]. These structural characteristics have also been supported by Raman spectra as shown in **Figure S5 (**in **SI)**. As it is seen from Raman spectra, 1LO and 2LO phonon modes are observed at 298 cm^{-1} and 587 cm^{-1} respectively. In addition to the LO phonons and their replicas, so other peaks are also found at 101 cm^{-1}, 162 cm^{-1}, 268 cm^{-1}, suggesting that

the nanorods have better crystal quality.[40]. Figure 2(e) shows the TEM image of CdS nanorods, where nanorods are cylindrical with smooth surface morphology. It is noted that the average diameter of nanorod is 120 nm and length is ~1 µm. The high-resolution TEM, as depicted in Figure 2(f,g), clearly indicates the single-crystalline nature of nanorods. However, the surface of nanorods consists of nanocrystals with a size of 5-6 nm, which is reflected in the SAED pattern of nanorod as shown in Figure 2(h).

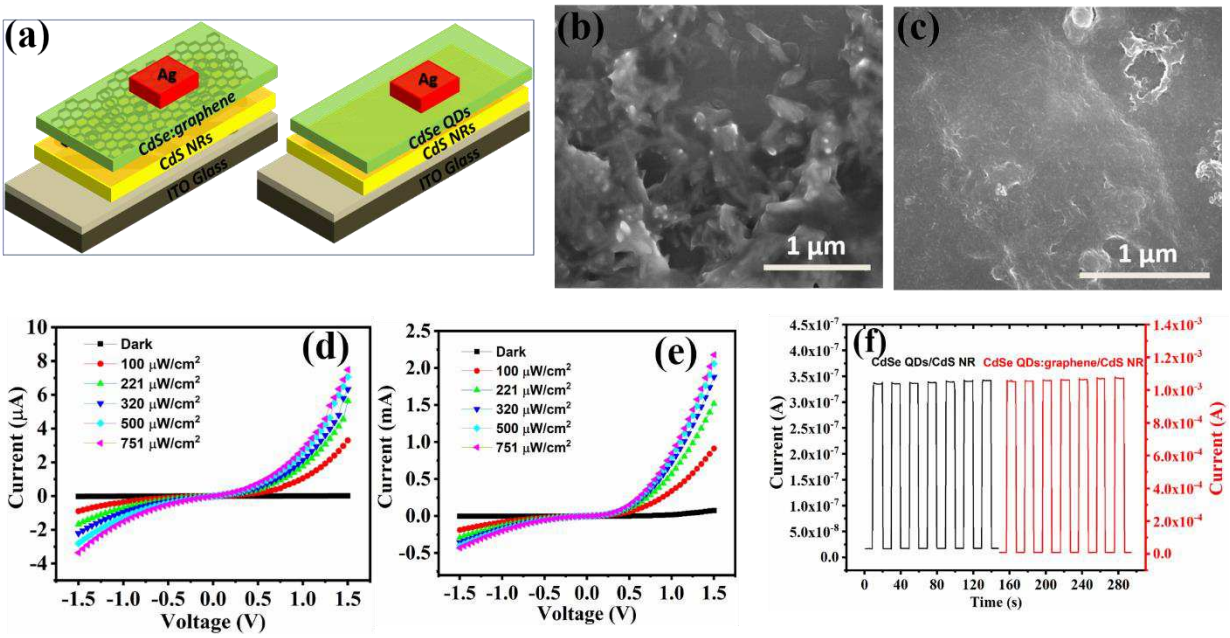

Figure.3 (a) Schematic diagram of the hybrid photodetector device structure. (b) FESEM image of CdS nanorods deposited on ITO/glass substrate. (c) CdSe QDs: graphene nanocomposite deposited on the CdS NRs/ITO/glass substrate. (d) I-V characteristics of the device with structure Ag/CdSe QDs/CdS NRs/ITO photodetector. (e) I-V characteristics of device with structure Ag/CdSe QDs:graphene/CdS NRs/ITO photodetector. (f) The I-t curve of photodetector under bias +1 V.

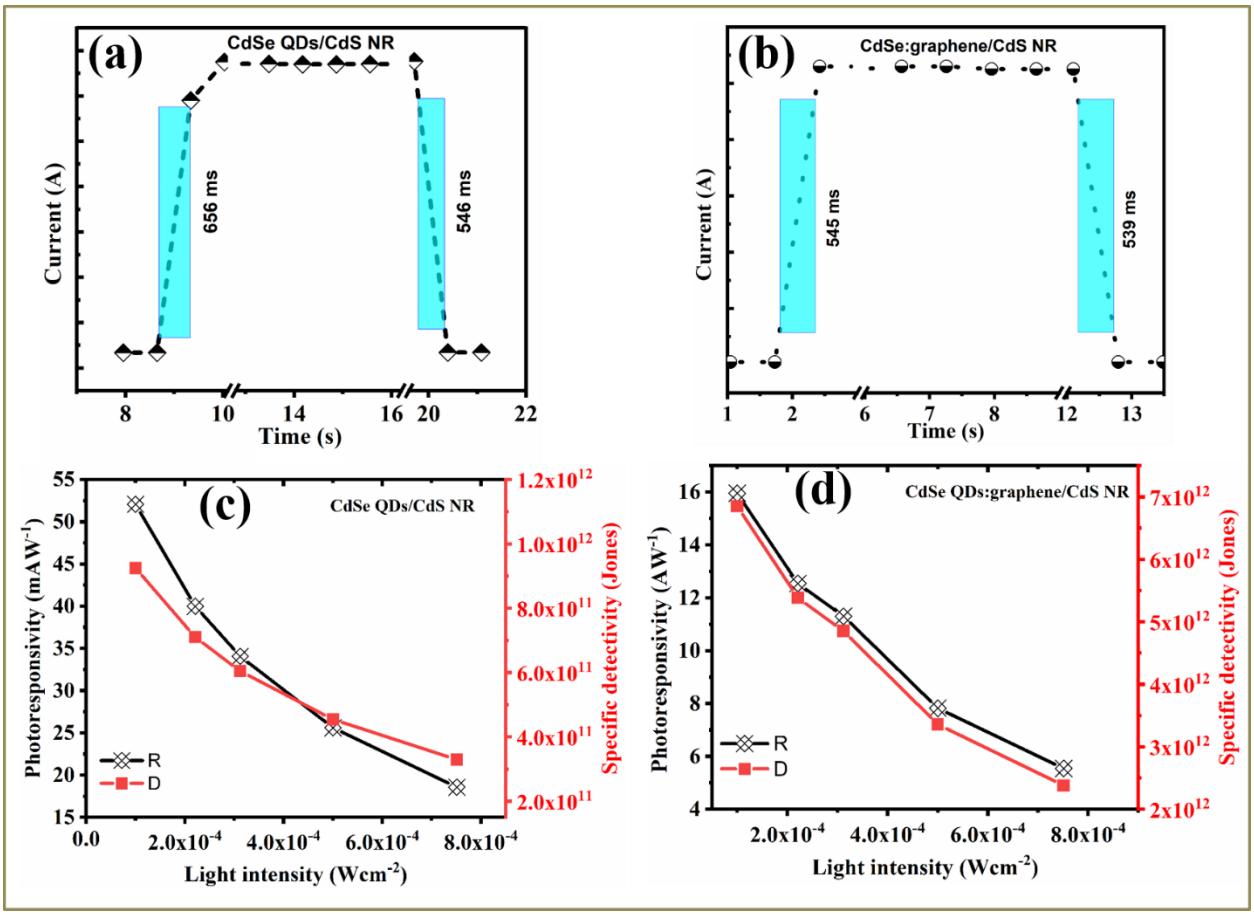

Figure.4 Temporal photoresponse of the heterojunction photodetector (a) device A. (b) device B. (c) Photoresponsivity and specific detectivity Vs light intensity for device A. (d) Photoresponsivity and specific detectivity Vs light intensity for device B.

To demonstrate the efficient charge transfer properties of nanohybrids, a heterojunction photodetector was fabricated with device structure as shown in Figure 3(a). Two types of the device have been fabricated such as ITO/CdSe/CdS/Ag (Device A) and ITO/graphene: CdSe /CdS/Ag (Device B). The surface morphology of drop-casted CdS NRs on ITO/glass substrates is shown in Figure 3(b) and also, dense and thick distribution of CdSe QDs: graphene nanocomposite film on CdS NRs is observed as shown in Figure 3(c). The photodetector device has been characterized by applying a bias sweep from +1.5 V to -1.5 V. Figure 3(d) shows the I-V curves of device A under 530 nm laser illumination at varied power from 100 $\mu W/cm^2$ to 751 $\mu W/cm^2$.

A clear rise of the photocurrent with increasing intensity of light was observed, indicating effective conversion of photon flux to photogenerated carriers. Moreover, the curve shows slight non-linear and asymmetrical behavior, confirming the proper formation of heterojunction. However, it was found that device B shows more non-linear characteristics compared to device A. It is noted that the dark current of device A and device B are 1.695×10^{-8} A and 9.91×10^{-6} A respectively. It clearly indicated that the dark current has been increased with graphene addition due to the increment of conductivity. At the same time, photocurrent was also increased tremendously with graphene doping from 1.0515 mA (100 $\mu W/cm^2$) to 2.799 mA (751 $\mu W/cm^2$). Moreover, the On-OFF switching of the device under +1 V bias is shown in Figure3(e), displaying stable and repetitive cycles illuminated with 530 nm and 100 $\mu W/cm^2$ light intensity, which demonstrating photodetection reversibility.

Another important characteristic of the photodetector is the linearity of photocurrent upon illumination light intensity. To examine such linearity relationship, 530 nm LED has been chosen with power variation from 100 $\mu W/cm^2$ to 751 $\mu W/cm^2$ at bias +1 V as shown in **Figure S6 (**in **SI)**. Fitting the plot with the power-law equation as $I_{ph}=AP^{\alpha}$, the value of α is 0.43 and 0.39 for device A and device B, respectively. The obvious deviation from the ideal value of 1 is attributed to the loss of photoexcited carriers through recombination. Both defects and impurities may act as charge recombination centers, which could be filled by photoexcited carriers as the light intensity increases. Moreover, the slight increase of α value indicates the inherent role of graphene as the electron collector and subsequent transportation.

Photoresponse time plays an important role in photodetector behavior. Figure4(a,b) shows the rise and decay time upon V_{bias}=+1 V for device A and device B under 530 nm illumination and 100 μWcm^{-2} light intensity. The rise time is defined as the time gap between 10 % of the “off” state to

90% of the “on” state and decay time is defined as the opposite. The decay time shows a slight decrement from 546 ms to 539 ms, while the rise time decreased from 656 ms to 545 ms after introducing graphene with CdSe QDs. Considering the fact that charge mobility in quantum dot films is limited by grain boundaries, the presence of graphene sheets provides an additional

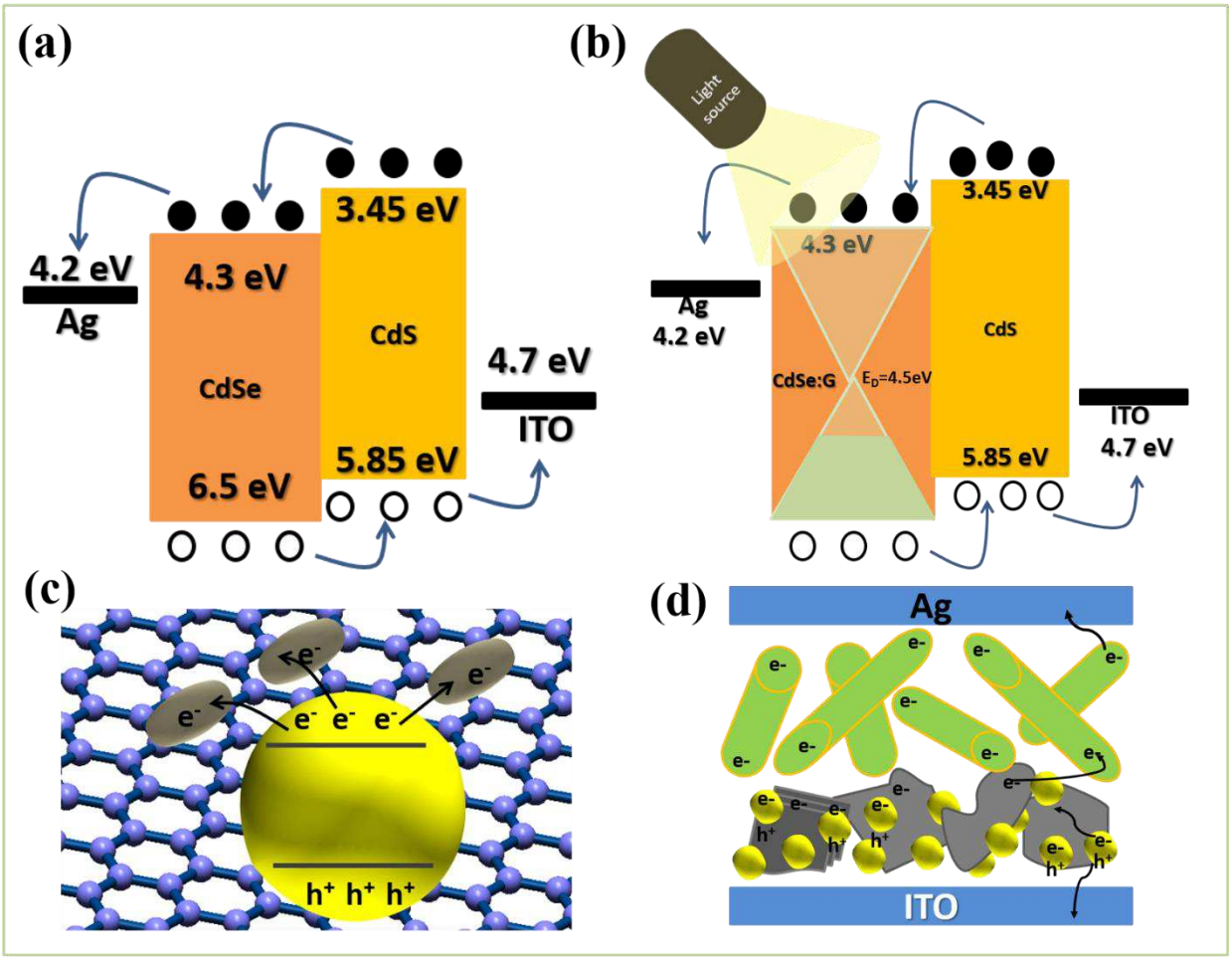

Figure.5 Schematic representation of charge carrier dynamics in (a) CdSe QDs/CdS NRs (device A) (b)CdSe QDs:Gr/CdS NRs (device B) (c) Excited state interaction between CdSe QDs and graphene. (d) shematics of charge carrier transportation in CdSe QDs:Gr/CdS NRs heterojunction photodetector.

conducting channel for charge transport[41, 42]. Therefore, device B shows better performance rather than device A.

Furthermore, the performance of photodetectors is evaluated in terms of key parameters such as photoresponsivity (R), Specific detectivity (D*), external quantum efficiency (EQE). The Photoresponsivity R is expressed as $R=I_p/PS$, where $I_p=I_{light}-I_{dark}$, P is the incident power density and S is the effective device area. D* is defined in terms of responsivity R and its simplified form is is $\boldsymbol{D^* = (I_p \sqrt{A}) / (P\sqrt{(2qI_d)})}$, where $I_p=I_{ph}-I_d$, A is the active area, P is the incident power density, q is the coulombic charge. As shown in Figure4c, the maximum photoresponsivity and specific detectivity for device A is calculated to be 18.57 mAW^{-1} and 9.24×10^{11} Jones respectively. On the other hand, device B shows an enhanced photoresponsivity and specific detectivity of 15.95 AW^{-1} and 6.85×10^{12} Jones respectively as depicted in Figure 4(d). Moreover, incident power-dependent R and D* indicate that R and D* have shown higher value at a weak light signal. Also, both R and D* decreased gradually with increasing the light intensity for both device A and device B. Therefore, the results strongly manifest the existence of considerable recombination loss of charge carriers in the device. This behavior has also been observed in other systems such as Gr/PbS, perovskite nanostructures, etc.[19, 43, 44].

Figure 5(a,b) shows a schematic diagram of the energy bands corresponding to the carrier transport mechanisms of the holes and electrons during light illumination for device A and device B. When a 530 nm light illuminates the photodetectors through the top electrode, the photons penetrate the CdSe QDs layer, resulting in the creation of the excitons. Because of the band alignment and potential difference between the band positions, the photo-generated electrons follow the heterojunction mechanism, where the electrons present in the CB of CdS NRs layer are transferred to the CB of CdSe QDs layer and to the Ag electrode and holes in the VB of CdSe QDs are transferred to VB of CdS NRs and to the ITO (Figure 5(a))[45]. On the other hand, in device B,

Table.1 Summary of key device performance parameters of this work and other reported graphene-QD based devices.

Device structure	Wavelength (nm)	Photoresponsivity R (AW^{-1})	Specific detectivity D* (Jones)	Rise/decay time (ms)	Ref.
Graphene/PbSe/TiO_2	350	0.506	3×10^{13}	0.003/0.053	[46]
Ge QDs:RGO/ZnO	1400	9.7	7.98×10^{12}	0.004/0.009	[47]
PET/graphene/CdS/Au	450	40	-	-	[48]
ZnO NWs/graphene/CdS	475	0.043	-	5/5	[49]
Graphene flake/ZnO nanotube	365	0.0022	-	68000/58000	[50]
InGaAs/Graphene	1550	7.6		0.0012/0.0096	[51]
$CsPbBr_3$/Graphene	405	3.4	7.5×10^{8}	7.9/125	[52]
Ag/CdSe QDs /CdS NRs/ITO	530	0.052	9.24×10^{11}	656/546	This work
Ag/graphene:CdSe QD/CdS NRs/ITO	530	15.95	6.85×10^{12}	545/539	This work

charge excitons are generated in the CdSe QDs: graphene nanocomposite under light illumination and charge carrier separation is occurred under applied electric field, however, in presence of graphene, charge carrier separation is enhanced due to nano heterojunction at the interface of CdSe QDs/graphene (Figure 5(c)). Besides, a higher conductive channel provided by graphene can induce the charge carrier transportation effectively. Therefore, the electrons and holes are accumulated at the Ag and the ITO layers, respectively, resulting in the generation of the photocurrent in the photodetectors (Figure.5 (d)). It is believed that the photodetector performance could be further improved by the proper ligand-exchange process to overcome the resistance provided by oleic acid and designing of the device structure. We also compared the performance of our device with other graphene nanocomposite-based photodetectors as shown in **Table 1.**

4. Conclusion

In summary, we have successfully synthesized the graphene: CdSe QDs nanocomposite at a low-temperature regime by a one-pot solvothermal method and subsequently demonstrated the heterojunction photodetector. It is found that the synergistic interaction between CdSe QDs and graphene facilitating the separation of electron-hole pairs and prolong the lifetime of the charge

carriers. Interestingly, the fabrication of heterojunction photodetector Ag/graphene: CdSe QDs/CdS NRs/ITO exhibits higher photoresponsivity and detectivity up to 15.95 AW^{-1} and 6.85×10^{12} Jones respectively. The appropriate structure and band alighnment in graphene:CdSe QDs/CdS NR heterojunction benefits the visible light absorption and enhanced charge transfer. The present study reveals that the formation of nano junction by introducing graphene into QD layers is a good strategy to improve the charge carrier separation and transportation that results in the enhancement of the photosensing capability of the photodetector.

Acknowledgments

This work was supported by the National Key Research and Development Program of China (Grant No. 2018YFB2200500), the National Natural Science Foundation of China (Grant no. 61974170,61934007,61675195), the Opened Fund of the State Key Laboratory of Integrated Optoelectronics No. IOSKL2018KF17, the Beijing Municipal Science and Technology Commission Project (Grant No. Z191100004819011).

Conflict of Interest

The authors declare no conflict of interest.

References

[1] Bonaccorso F, Sun Z, Hasan T and Ferrari A C 2010 *Nat.Photonics.,* **4** 611-22

[2] Reddy D, Register L F, Carpenter G D and Banerjee S K 2011 *J.Phys D.Appl.Phys.,* 44 313001

[3] Freitag M, Low T, Xia F and Avouris P 2013 *Nat.Photonics.,* **7** 53-9

[4] Liu J-Y, Li X-X, Huang J-R, Li J-J, Zhou P, Liu J-H and Huang X-J 2017 *J.Mater.Chem A.,* **5** 5977-94

[5] Danielson E, Sontakke V A, Porkovich A J, Wang Z, Kumar P, Ziadi Z, Yokobayashi Y and Sowwan M 2020 *Sens Actuators B Chem.,* **320** 128432

[6] Akbari-Sharbaf A, Ezugwu S, Ahmed M S, Cottam M G and Fanchini G 2015 *Carbon,* **95** 199-207

[7] Khan M, Tahir M N, Adil S F, Khan H U, Siddiqui M R H, Al-warthan A A and Tremel W 2015 *J.Mater.Chem A.,* **3** 18753-808

[8] Song X, Zhang Y, Zhang H, Yu Y, Cao M, Che Y, Dai H, Yang J, Ding X and Yao J 2017 *Nanotechnol.,* **28** 145201

[9] Murray C B, Norris D J and Bawendi M G 1993 *J.Am.Chem.Soc.,* **115** 8706-15

[10] Pu Y, Cai F, Wang D, Wang J-X and Chen J-F 2018 *Ind.Eng.Chem.Res.,* **57** 1790-802

[11] Wu J, Chen S, Seeds A and Liu H 2015 *J.Phys D.Appl.Phys.,* **48** 363001

[12] Li J and Zhu J-J 2013 *Analyst* **138** 2506-2515

[13] Zhao N, Osedach T P, Chang L-Y, Geyer S M, Wanger D, Binda M T, Arango A C, Bawendi M G and Bulovic V 2010 *ACS Nano* **4** 3743-3752

[14] Tong L, Qiu F, Zeng T, Long J, Yang J, Wang R, Zhang J, Wang C, Sun T and Yang Y 2017 *RSC Adv.,* **7** 47999-8018

[15] Guo C X, Yang H B, Sheng Z M, Lu Z S, Song Q L and Li C M 2010 *Angew.Chem.Int*., **49** 3014-3017

[16] Goossens S, Navickaite G, Monasterio C, Gupta S, Piqueras J J, Pérez R, Burwell G, Nikitskiy I, Lasanta T, Galán T, Puma E, Centeno A, Pesquera A, Zurutuza A, Konstantatos G and Koppens F 2017 *Nat.Photonics.,* **11** 366-371

[17] Geng X, Niu L, Xing Z, Song R, Liu G, Sun M, Cheng G, Zhong H, Liu Z, Zhang Z, Sun L, Xu H, Lu L and Liu L 2010 *Adv.Mater.,* **22** 638-42

[18] Kim Y-T, Han J H, Hong B H and Kwon Y-U 2010 *Adv.Mater.,* **22** 515-518

[19] Sun Z, Liu Z, Li J, Tai G-a, Lau S-P and Yan F 2012 *Adv.Mater.,* **24** 5878-5883

[20] Chen W, Ahn S, Balingit M, Wang J, Lockett M and Vazquez-Mena O 2020 *Nanoscale.,* **12** 4909-4915

[21] Cook B, Gong M, Corbin A, Ewing D, Tramble A and Wu J 2019 *ACS Omega* **4** 22497-22503

[22] Zhang B, Wang K, Chang R, Yi X, Zhang Y and Wang S 2019 *J.Phys.Chem C.,* **123** 24943-24948

[23] Zedan A F, Sappal S, Moussa S and El-Shall M S 2010 *J.Phys.Chem C.,* **114** 19920-19927

[24] Miao X, Gosztola D J, Sumant A V and Grebel H 2018 *Nanoscale.,* **10** 7040-6

[25] Cao S, Wang J, Ma F and Sun M 2018 *Nanotechnol.,* **29** 145202

[26] Cao A, Liu Z, Chu S, Wu M, Ye Z, Cai Z, Chang Y, Wang S, Gong Q and Liu Y 2010 *Adv.Mater.,* **22** 103-6

[27] Konstantatos G, Badioli M, Gaudreau L, Osmond J, Bernechea M, de Arquer F P G, Gatti F and Koppens F H L 2012 *Nat.Nanotechnol.,* **7** 363-8

[28] Siy J T, Brauser E H, Thompson T K and Bartl M H 2014 *J.Mater.Chem C.,* **2** 675-82

[29] Yükselici M H, Aşıkoğlu Bozkurt A and Ömür B C 2013 *Mater. Res.Bull.,* **48** 2442-9

[30] Yoon D, Moon H, Son Y-W, Choi J S, Park B H, Cha Y H, Kim Y D and Cheong H 2009 *Phys.Rev B* **80** 125422

[31] Ni Z H, Yu T, Lu Y H, Wang Y Y, Feng Y P and Shen Z X 2009 *ACS Nano* **3** 483-

[32] Calizo I, Balandin A A, Bao W, Miao F and Lau C N 2007 *Nano Lett.,* **7** 2645-2649

[33] Ren Z, Yu J, Pan Z, Wang J and Zhong X 2017 *ACS Appl.Mater.Interfaces.,* **9** 18936-44

[34] Jung M-H and Chu M-J 2014 *Nanoscale.,* **6** 9241-9

[35] Tang X, Zu Z, Zang Z, Hu Z, Hu W, Yao Z, Chen W, Li S, Han S and Zhou M 2017 *Sens Actuators B Chem.,* **245** 435-40

[36] Zhang H, Lv X, Li Y, Wang Y and Li J 2010 *ACS Nano* **4** 380-6

[37] Yan P, Xie Y, Qian Y and Liu X 1999 *Chem.Commun.,* 1293-4

[38] Yang J, Zeng J-H, Yu S-H, Yang L, Zhou G-e and Qian Y-t 2000 *Chem.Mater.,* **12** 3259-63

[39] Ascencio J A, Santiago P, Rendón L and Pal U 2004 *Appl.Phys.A.,* **78** 5-7

[40] Hu C, Zeng X, Cui J, Chen H and Lu J 2013 *J.Phys.Chem C.,* **117** 20998-1005

[41] Koleilat G I, Levina L, Shukla H, Myrskog S H, Hinds S, Pattantyus-Abraham A G and Sargent E H 2008 *ACS Nano* **2** 833-40

[42] Kamat P V 2010 *J.Phys.Chem.Lett.,* **1** 520-7

[43] Ahn S, Chen W, Moreno-Gonzalez M A, Lockett M, Wang J and Vazquez-Mena O 2020 *Adv.Elect.Mater.,* **6** 2000014

[44] Chandrasekar P V, Yang S, Hu J, Sulaman M, Shi Y, Saleem M I, Tang Y, Jiang Y and Zou B 2019 *Nanoscale.,* **11** 5188-96

[45] Skromme B J and Sujan G K 2018 *Reference Module in Materials Science and Materials Engineering*: Elsevier.

[46] Manga K K, Wang J, Lin M, Zhang J, Nesladek M, Nalla V, Ji W and Loh K P 2012 *Adv.Mater.,* **24** 1697-702

[47] Liu X, Ji X, Liu M, Liu N, Tao Z, Dai Q, Wei L, Li C, Zhang X and Wang B 2015 *ACS Appl.Mater.Interfaces.,* **7** 2452-8

[48] Chan Y, Dahua Z, Jun Y, Linlong T, Chongqian L and Jun S 2020 *Physica E Low Dimens.Systs.Nanostruct.,* **124** 114216

[49] Huang G, Zhang P and Bai Z 2019 *J.Alloys.Compd.,* **776** 346-52

[50] Huang B-R, Saravanan A and Lu H-C 2020 *Adv.Mater.Interfaces*., **7** 1901694

[51] Yang Q, Wu Q, Luo W, Yao W, Yan S and Shen J 2019 *Mater.Res.Express.,* **6** 116208

[52] Che Y, Cao X, Zhang Y and Yao J 2021 *J.Mater.Sci.,* **56** 2341-6

Figures

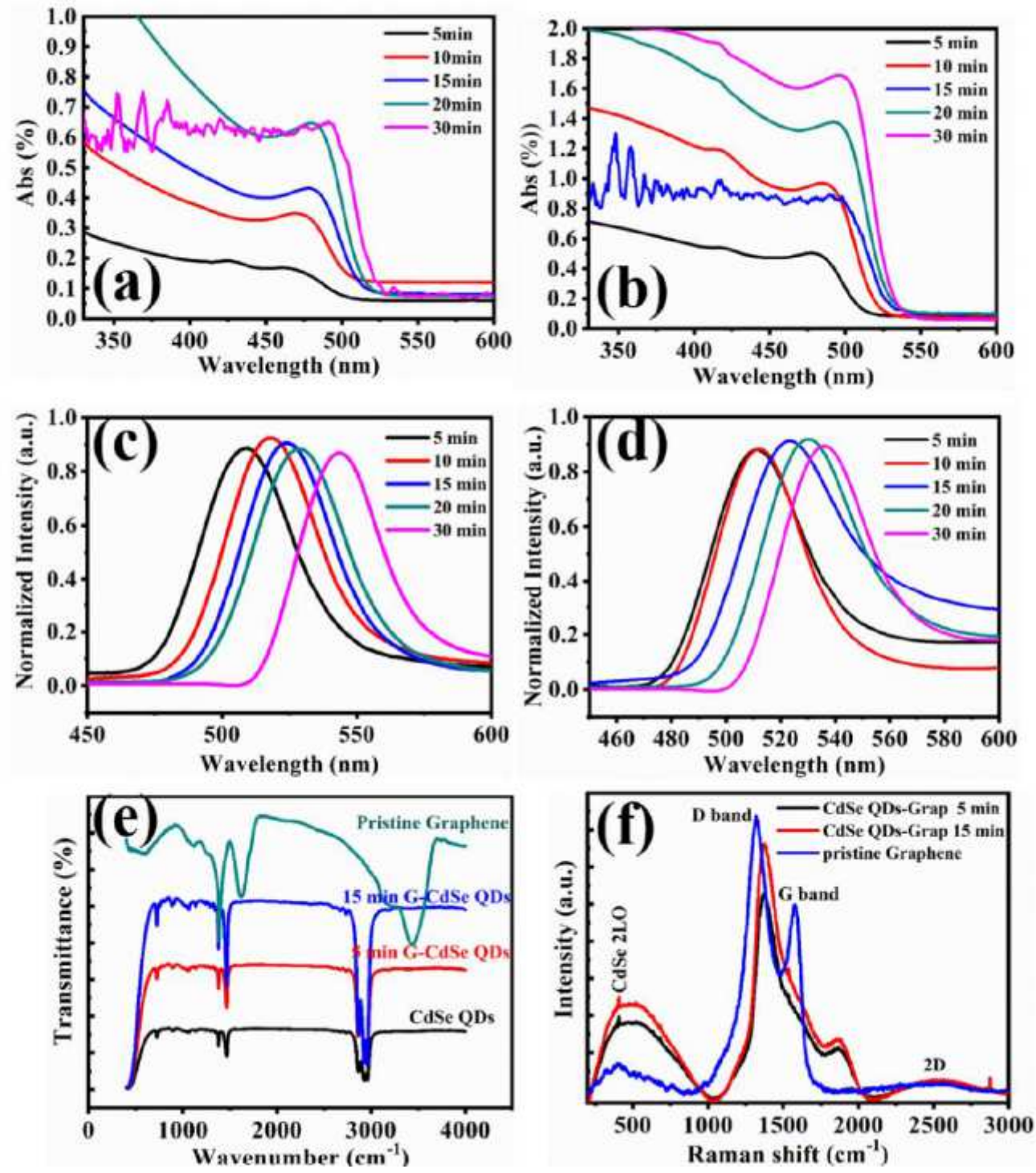

Figure 1

UV-visible absorption spectra spectra of (a) CdSe QDs (b) graphene:CdSe QDs. Photoluminescence spectra of (c) CdSe QDs (d) graphene:CdSe QDs. (e) FTIR spectra of pure CdSe QDs, graphene: CdSe QDs synthesized for 5 min, graphene: CdSe QDs synthesized for 15 min, and pure graphene. (f) Raman

spectra of the pristine graphene, graphene: CdSe QDs synthesized for 5 min, and graphene: CdSe QDs synthesized for 15 min.

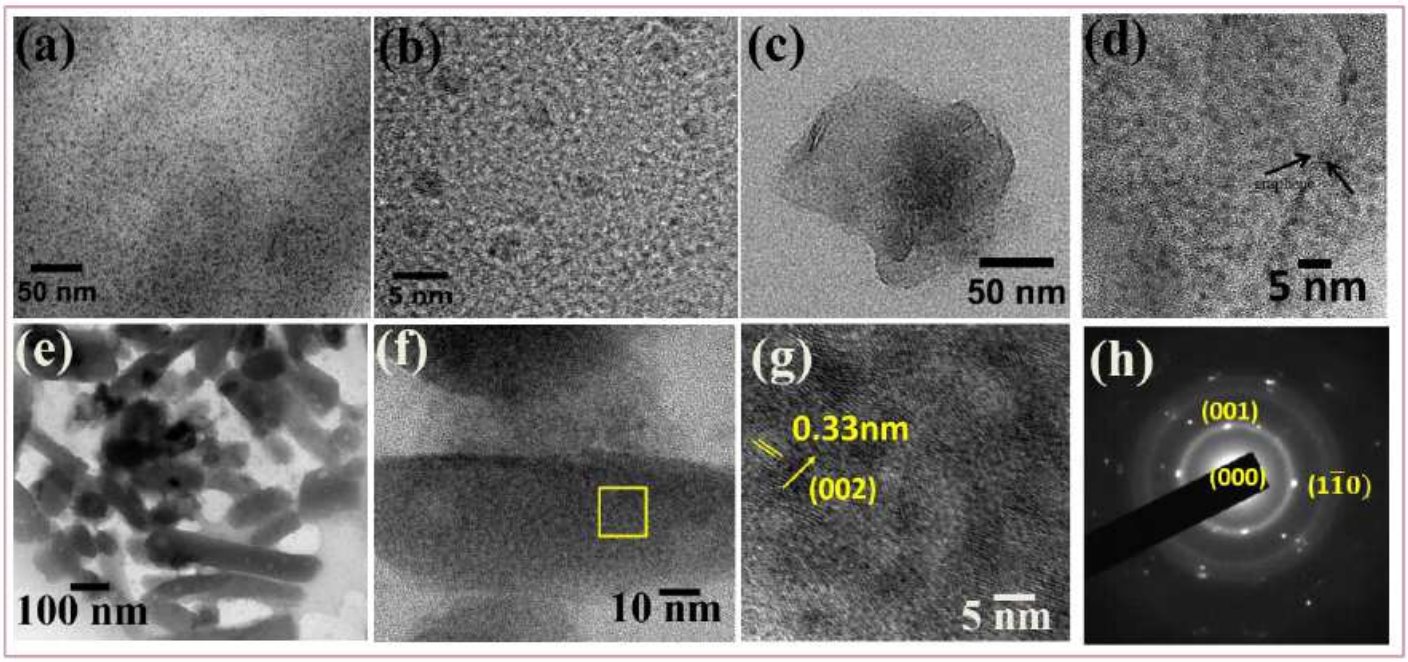

Figure 2

(a) Low magnified TEM image of CdSe QDs. (b) High magnification TEM image of CdSe QDs. (c) HRTEM image of graphene-CdSe QDs nanocomposite. (d) high magnification HRTEM image of graphene- CdSe QDs. (e) Low magnification TEM image of CdS nanorods. (f) high magnification TEM image of CdS nanorod. (g) the enlarged portion of the selected area in CdS nanorods (yellow square in Figure2(f)). (h) selected area electron diffraction (SAED) pattern of CdS nanorods.

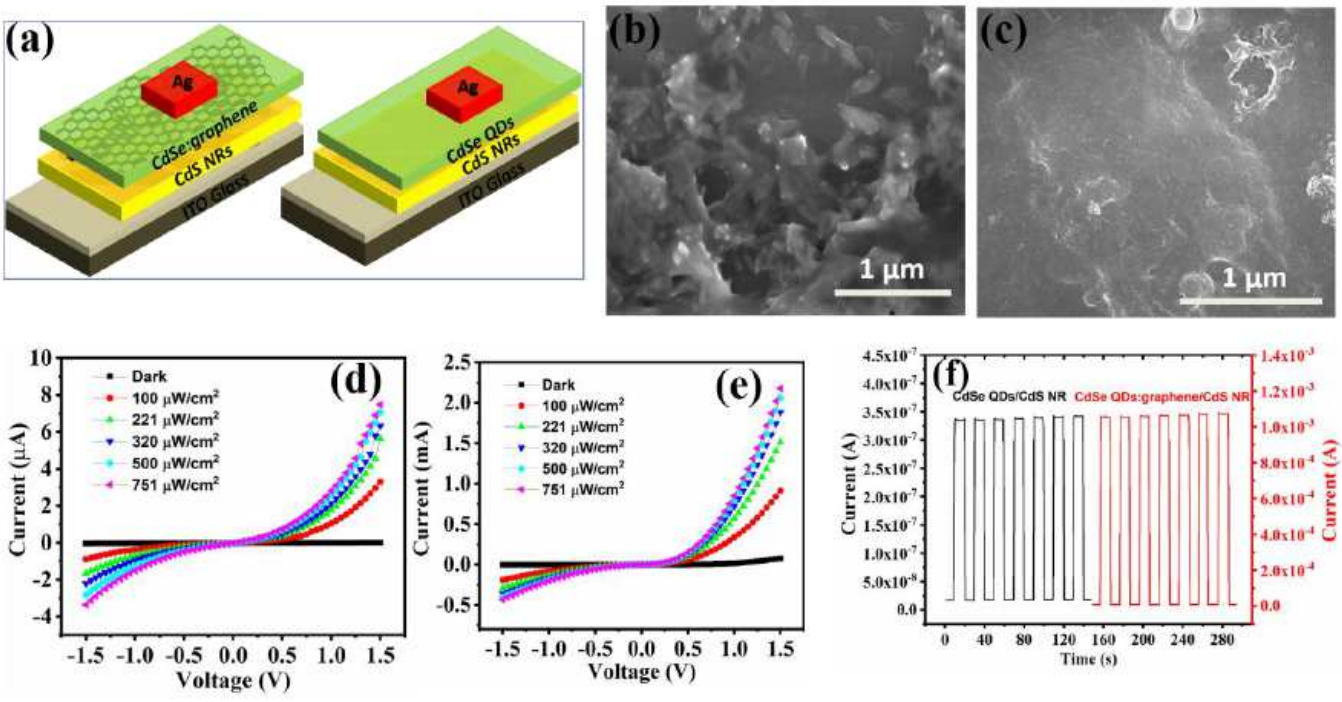

Figure 3

(a) Schematic diagram of the hybrid photodetector device structure. (b) FESEM image of CdS nanorods deposited on ITO/glass substrate. (c) CdSe QDs: graphene nanocomposite deposited on the CdS NRs/ITO/glass substrate. (d) I-V characteristics of the device with structure Ag/CdSe QDs/CdS NRs/ITO photodetector. (e) I-V characteristics of device with structure Ag/CdSe QDs:graphene/CdS NRs/ITO photodetector. (f) The I-t curve of photodetector under bias +1 V.

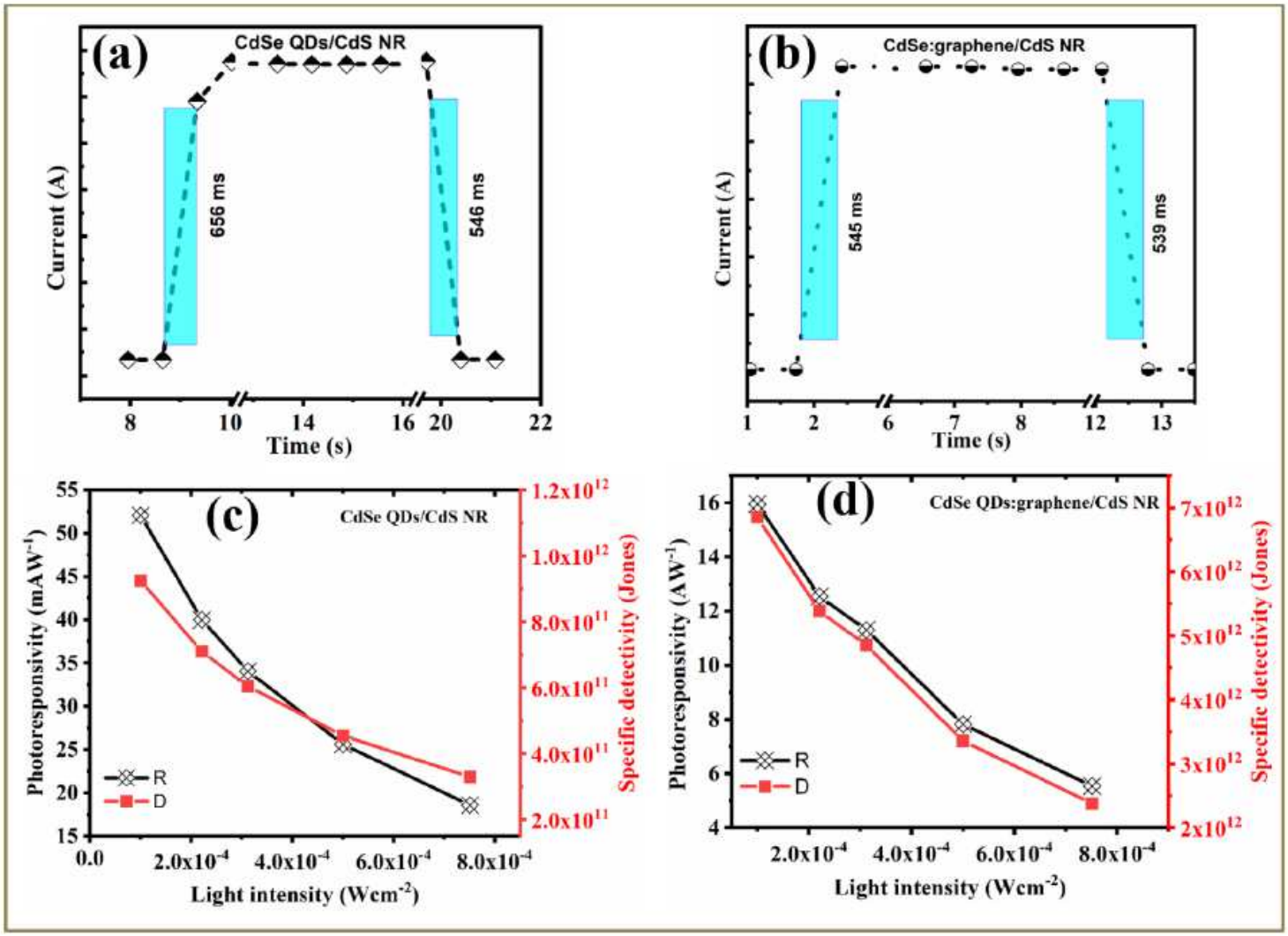

Figure 4

Temporal photoresponse of the heterojunction photodetector (a) device A. (b) device B. (c) Photoresponsivity and specific detectivity Vs light intensity for device A. (d) Photoresponsivity and specific detectivity Vs light intensity for device B.

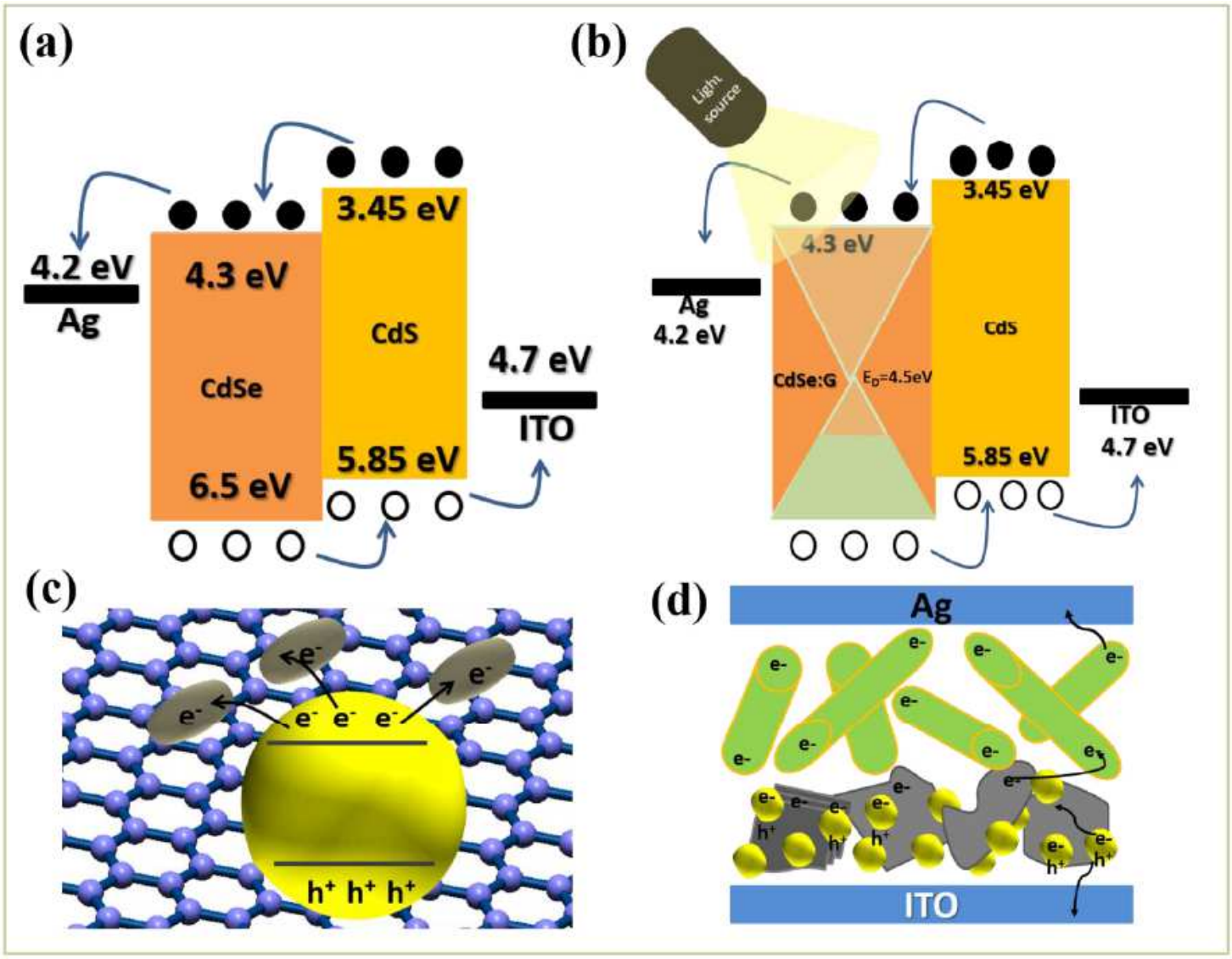

Figure 5

Schematic representation of charge carrier dynamics in (a) CdSe QDs/CdS NRs (device A) (b)CdSe QDs:Gr/CdS NRs (device B) (c) Excited state interaction between CdSe QDs and graphene. (d) shematics of charge carrier transportation in CdSe QDs:Gr/CdS NRs heterojunction photodetector.

Supplementary Files

This is a list of supplementary files associated with this preprint. Click to download.

- SupportingInformation.docx